Report 73-3

January 1973

A COMPARISON OF THE TIME VARIATION OF SEVERE STORM ENERGETICS AS ESTIMATED FROM RADAR OBSERVATIONS VERSUS A NUMERICAL EXPERIMENT

By: D. N. Sikdar, R. E. Schlesinger and C. E. Anderson

Prepared for:
National Science Foundation

Grant No. GI-31278X

C. E. Anderson, Principal Investigator
D. N. Sikdar, Co-Principal Investigator

Department of Meteorology

University of Wisconsin

Madison, Wisconsin 53706

A Comparison of the Time Variation of Severe Storm Energetics As Estimated From Radar Observations Versus a Numerical Experiment

D. N. Sikdar, R. E. Schlesinger and C. E. Anderson

Department of Meteorology and Space Science and Engineering Center
The University of Wisconsin
Madison, Wisconsin

ABSTRACT

The time variation of mass-integrated liquid water and latent heat release for a severe thunderstorm in marked vertical wind shear is investigated for an actual Oklahoma storm and for a two-dimensional numerical modeling experiment.

For the actual storm, an approximate continuity equation for liquid water variation is used together with profiles of radar reflectivity. Empirical relationships are utilized for reflectivity and liquid water content, as well as for rainfall rate and downdraft evaporation rate. Estimates of the parameters in question are then readily obtained by treating reflectivity contours as cylindrical shells.

To estimate these parameters from the numerical model, the two-dimensional cloud is extended to a three-dimensional region whose horizontal cross-sections are ellipses approximating typical observed shapes. At each level, horizontal averages of relevant integrands are assumed equal to those in the model plane.

It is found on the basis of these analyses that at maturity, the actual storm and the model storm exhibit comparable magnitudes with respect to both parameters. Time variation is smoother in the model than in the real storm, probably due mainly to limitations on grid resolution.

1. Introduction

The water and energy budgets of severe storms have been of interest since Braham (1952), utilizing data from the Thunderstorm Project (Byers and Braham, 1949), attempted to evaluate various components of thunderstorm energetics and found the latent heat release to be the major source. However, the Ohio storms investigated in the Project were airmass-type and relatively short-lived. A large hailstorm exhibits a quasi-steady mature state lasting for a few hours, possibly as a single "supercell". Energetically, these storms are exceedingly active and process much more water vapor than an ordinary Ohio storm. The latent heat release in an ordinary storm is about 5×10^{11} cal sec^{-1} (Braham, 1952) while in a severe storm it may be in excess of 8×10^{12} cal sec^{-1} (McLaughlin, 1967), at least an order of magnitude higher.

While various investigators have studied severe storm energetics at a particular time and place, very little progress has been made in regard to their time variations because of the hazards and difficulties involved in frequently sampling the interior of the storm by airborne sensors. In recent years, however, remote sensing of the water budget in severe storms has been made possible by calibrated weather radars utilizing relationships between the cloud liquid water content and the radar reflectivity profiles as a function of time. The time lapse echo contour displays in CAPPI (constant altitude plan position indicator) mode essentially provide such information. Using such a concept Barge (1968) estimated the latent heat released for the duration of four severe storms near Montreal and found the energy output to range from one to three orders of magnitude higher than for a moderate storm.

The purpose of this paper is two-fold: first, to find out the nature of the time varying water and energy budgets of a typical severe storm as

deduced from radar data; second, to compare these observed magnitudes with those obtained from a two-dimensional numerical simulation experiment.

2. An Approximate Scheme for Computing From Observed Data

One can visualize a severe storm as consisting of two regions: a core where air is ascending or descending without mixing (no entrainment), and a shell of cloud debris nearly at rest. The primary source of water vapor for a storm is the inflow of moist air through the cloud base while the secondary source is lateral entrainment. Physically one can picture the evolution processes of a storm fed continuously by moist air which ascends through the updraft into the core. A part of the cloud is stored in the core and is evaporated later in the downdraft; a second part evaporates in the shell, due to horizontal advection of dry air into the storm, and a third part falls out as precipitation. A weather radar is capable of detecting these changes in terms of precipitable water content as the storm evolves. However, some of the liquid droplets may not attain radar-detectable size, may be stored as cloud droplets, or may escape as ice crystals through the top of the storm so that latent heat release computed from radar data will be an underestimate.

In radar studies of storms, the PPI observations are taken more frequently than the RHI (range-height indicator). Unfortunately for the storm selected for this study, some problems with the signal integrator of the PPI radar system resulted in underestimates of the radar reflectivity values (Wilson, 1969), so that the RHI data obtained from an MPS-4 had to be used. In the RHI reflectivity profile, cylindrical symmetry of reflectivity (Z_e, $mm^6\ m^{-3}$) contours has been assumed through the storm depth to provide easy computation of the volume of each inner shell bounded by the radar beam width (Figure 1) and therefore of the volume-integrated liquid water content along a particular azimuth of a storm as a function of time. The physical significance of this assumption implies a constant distribution of ΣND^6 with height where N is the

drop concentration; D is the diameter of the water droplets and the summation extends over the droplet size spectrum in a unit volume. To further simplify the model, all water content is assumed to be in liquid form regardless of altitude.

In computing the time variations of latent heat release from the radar reflectivity profiles the following basic steps are involved:

1) To establish a reflectivity-rainfall relationship,

2) To establish a reflectivity-liquid water content relationship, in which it is assumed that the drop size distribution in the storm follows previously observed laws,

3) To solve a continuity equation for radar-detectable liquid water content on the basis of steps 1 and 2.

It should be pointed out here that the volume sampled by the radar beam (Figure 1) could be less than the total volume of the storm and therefore, the estimates of liquid water content could be less than actual; however, since we are mostly concerned with the time variation of the liquid water content and not in the absolute magnitude, our estimates on the generation term in the budget equation (5) should be correct at least within an order of magnitude.

3. Data Source and Analysis Technique

Radar and rainfall data were obtained from the National Severe Storms Laboratory (NSSL), which has a 10 cm WSR-57 radar at Norman, Oklahoma with a peak transmission power of 0.5 megawatt and a 2° conical beam width. The PPI photographs obtained from it show reflectivities at intervals of 10 db with ±3 db calibration accuracy. Supplementing this is an MPS-4 RHI radar (1.4° conical beam) calibrated to read reflectivities at 10 dbz intervals, depicting the vertical distribution of liquid water.

A surface meso-network covering approximately 5500 mi^2 provides all standard meteorological parameters (Barnes, 1971).

a. Some features of the selected storm

The storm analyzed in this study occurred on 23-24 May 1968 within the radar range of Norman. In regard to the synoptic situation, the 1200 GMT chart indicated a weak quasi-stationary front oriented NE-SW across central Oklahoma; at 500 mb a long-wave trough was present in the western Rockies with south-westerly flow over Oklahoma. The movement of a short-wave trough into Oklahoma from the Texas panhandle and an incursion of warm moist air from the Gulf of Mexico (dew point temperature about 69°F) at lower levels were conducive to explosive development of a few convective cells by late afternoon.

A strong convective cell intensified rapidly by 1900 CST to the southwest of the existing cells in the southeastern portion of the NSSL meso-network. Severe weather reports included a funnel cloud southwest of Paul's Valley at 1019 CST along with 3/4 to 1 1/2-in hail from 1936 to 2000, between Wynnewood and Davis, Oklahoma (1968 storm data, NOAA). The storm trajectory through the surface meso-network is shown in Figure 2. The hodograph shown in the inset exhibits pronounced wind shear in the vertical and the storm appears to have

moved to the right of the upper winds. The PPI and RHI histories of the storm are shown in Figure 3. The area of the storm increased significantly on the PPI scope after its merger with a nearby cell around 1845 CST. An indentation (see arrow) to the south of the storm became very pronounced between 1900 and 1930 on the PPI indicating a probable location of the weak echo region (Marwitz, 1972). On the RHI time section in Figure 3, this strong updraft region appeared as a notch in the southeast sector of the storm (see arrow).

b. Rainfall analysis and radar reflectivity profiles

Of the various water sources and sinks, only the rainfall can be measured with high accuracy. Accordingly, the radar reflectivity profiles were first calibrated against the rainfall rates obtained from the NSSL meso-network. The rainfall rates R (mm hr^{-1}) were computed directly from the recording raingauge strip charts and the reflectivity Z_e (mm^6 m^{-3}) over the raingauges at the same time from the radar photographs.

Figure 4 presents the time variations of the rainfall rate during the life cycle of the severe storm under study. The rainfall varied from 7×10^5 to more than 4×10^6 kg sec^{-1}, in reasonable agreement with values obtained for severe storms (Geotis, 1971; Fankhauser, 1971; McLaughlin, 1967) using Z-R relationships. Four prominent peaks separated by 15 to 25 minutes are apparent in this diagram. The first maximum around 1840 CST may be attributed to the merger with an adjoining cell. Funnel clouds and large hail were reported 10 to 15 minutes after the second and third maxima, respectively.

c. Radar Reflectivity Profiles and Liquid Water Content

Empirical relations relating the radar-reflectivity, Z_e (mm^6 m^{-3}), M (the concentration of liquid water, gm m^{-3}) and R (precipitation rate), have been worked out in the past. In this report we have used the expression for rain

after Gunn and Marshall (1958), namely,

$$Z_e = 2.39 \times 10^4 M^{1.82} \quad [mm^6 m^{-3}] \tag{1}$$

In the absence of any measurements of drop-size distribution in the severe storm investigated, this empirical equation appeared to be the only choice.

The scheme employed for computing the total liquid water content of the storm as a function of time is as follows:

a. Volume of a shell bounded by two adjacent reflectivity contours, (Z_{e1}, Z_{e2}) and radar beam-width, θ (radar beam completely filled), is first determined from the RHI reflectivity profiles (sample shown in Figure 3).

$$V_i(Z_{e1},Z_{e2}) = \bar{R}\cdot\theta\cdot[h_{\bar{R}}(R_2-R_1) - h_{\bar{r}}(r_2-r_1)] \tag{2}$$

where R is the range in nautical miles and h is the height of the echo top at the mean R in kilofeet; r refers to the second contour.

b. Liquid water content (LWC) in the shell is obtained using the Gunn-Marshall (1958) equation:

$$LWC = 3.93 \cdot 10^{-3} \bar{Z}_e^{0.55} \cdot V_i(Z_{e1},Z_{e2}) \tag{3}$$

where

$$\bar{Z}_e = (Z_{e1} + Z_{e2})/2$$

c. $$\text{Total LWC} = K \sum_{i=1}^{5} LWC \tag{4}$$

where K is a constant accounting for various conversion factors; i varies through 5 shells in steps of 10 dbz.

The total radar-detectable liquid water content thus derived is presented in Figure 5. The total liquid water content, as one would expect, increased

rapidly during the early stages of the storm, reaching a maximum of 5.7×10^8 kg around 1920 CST. This is at least one order of magnitude higher than estimates provided by Braham (1952) for a moderate thunderstorm.

4. Water and Energy Budgets of the Storm

The rate of condensation in the storm has been computed from a continuity equation for radar-detectable liquid water content similar to one used by Holtz (1968):

$$\frac{dW}{dt} = G - R - E \qquad (5)$$

where W is the total radar-detectable liquid water content of a storm, E the evaporation rate in the downdraft, G the condensation rate in the updraft, and R the rainfall rate.

The term dW/dt can be directly obtained by finite differences from Figure 5, while the rainfall rate R can be obtained from Figure 4. A problem arises with the estimation of E, as this component is difficult to measure. However, previous investigators (Braham, 1952; McLaughlin, 1967), deriving this term as a residual in their water balance equations, have found it to be of the same order of magnitude as R. In his analysis of a severe storm in Oklahoma, the area involved in this study, McLaughlin found that the evaporation rate at peak storm intensity was two-thirds the rainfall rate. Accordingly, this approximation has been used here for the duration of the storm, simplifying the budget equation (5).

The resulting generation rate G thus obtained (Figure 6a) showed a few peaks with the highest one (8×10^6 kg sec^{-1}) near 1920 CST, about 10 minutes before the large hailfall from the storm was reported. The peak of 6.7×10^6 kg/sec around 1850 CST may be attributed to the merging of the storm with an adjacent cell. The other peaks in the fluctuation of storm energetics, e.g. at 1825 CST and 1945 CST, are likely due to regeneration of the severe storm activity with the growth of new cells in the complex.

The conversion rate G when multiplied by the heat of vaporization at 0°C (597 cal gm^{-1}) yields the equivalent latent heat release. In Figure 6b, a maximum value of nearly 4.7×10^{12} cal sec^{-1} (equivalent to 1.7×10^{7} megwatts) is obtained. This is more than an order of magnitude higher than for a moderate thunderstorm (Braham, 1952) and in excellent agreement with values obtained by other investigators (McLaughlin, 1967; Brown, 1967; Geotis, 1971; Sikdar et al., 1970). Thus we may safely assume that our subject storm is typical of severe storms in respect to the magnitude of energy release and its time variability.

5. A Comparison Between Observations and the Numerical Model

a. Background

In a previous paper, Schlesinger (1972) used a two-dimensional anelastic numerical model with vertical shear to analyze the time variation of net transformation rates for several types of energy over a fixed open rectangular region through which a convective storm propagated while maturing. However, the main area of interest was the relative importance of the various physical processes contributing to net transformation rates, rather than actual magnitudes. Energy per unit mass was weighted over the domain, of which the cloud occupied only a small fraction until well into maturity. In particular, processes confined to the cloud were not evaluated in a fashion readily applicable to direct comparison with the types of observations described in Section 3 and 4.

An attempt has been made here to estimate latent heat release and total masses of liquid water and precipitation by visualizing the plane of the model as a plane of symmetry and assuming a specific shape for the storm in horizontal planes normal to it. With its rectangular geometry, the model most nearly simulates a vertical cross-section of an infinitely long squall line. However, previous estimates of latent heat release in actual severe storms have involved individual storms rather than squall lines taken as single entities. Therefore, for present purposes, the cloud outline in the two-dimensional model is treated as the vertical cross-section for a finite three-dimensional cloud, even though a truly three-dimensional model might have yielded considerably different point-by-point configurations and time dependencies.

b. List of symbols

For describing the method of estimation, the following symbols will be helpful:

ρ air density

c_p specific heat at constant pressure for air (1.004×10^3 m^2 sec^{-2} C^{-1})

γ_d dry-adiabatic lapse rate (9.77×10^{-3} C m^{-1})

γ_m moist-adiabatic lapse rate

w vertical velocity of air

L liquid water content

L_p precipitation content

i horizontal grid index ($1 \leq i \leq M$)

j vertical grid index ($1 \leq j \leq N$)

Q unspecified variable

n_j number of consecutive grid points at the jth grid level across a region of cloud or precipitation

Δx horizontal grid separation

Δz vertical grid separation

A_j assumed horizontal cross-sectional area for cloud or precipitation slice at jth level

R unspecified region

$I_R(Q)$ $\iiint Q \, dz \, dy \, dx$

$\tilde{Q}_j$ $(1/n_j) \sum_i Q_{i,j}$ where i sweeps across a region of cloud or precipitation with the grid

σ_j weighting factors (1/2 for j = 1 and j = N, 1 otherwise)

c. Assumptions

1) SOME FEATURES OF THE MODEL

In the present context, the following features of the model should be noted:

1) The ice phase and latent heat of fusion are not explicitly included.

2) Saturated ascent and descent are assumed moist-adiabatic, temperature changes being computed with the formula used by Murray and Anderson (1965).

3) An instantaneous local phase adjustment is made in two possible cases. Any supersaturation is removed by release of latent heat, and any liquid water in unsaturated air evaporates until the wet-bulb temperature is reached or all liquid water is consumed.

4) After application of the local adjustment wherever necessary, all grid points with liquid water are saturated with vapor. Liquid water is partitioned into cloud droplets, assumed to have zero relative fall speed, and precipitation particles, using a simplified approach due to Takeda (1966). Until the cloud top reaches the -20C level, all liquid water exists as cloud droplets. Thereafter, all liquid water above 1 gm m^{-3} is assumed to be precipitation, and the remainder is cloud droplets. In Takeda's approach, relative fall speed is assumed to be a function of precipitation content, proportional to the square root of precipitation content up to 4 gm m^{-3} but equal to 9 m sec^{-1} for all greater content values.

2) ESTIMATION OF MASS-INTEGRATED QUANTITIES

The following assumptions have been made for estimating mass-integrated quantities for ready comparison with observations:

1) Each hypothetical cloud slice is elliptical, with major axis in the model plane (x-z) and minor axis one-half as long in the x-y plane. The same assumption is made for precipitation regions. The assumed shape (Figure 7) is reasonably well motivated by satellite observations (for cirrus canopies generated by storms) and PPI radar echoes for sheared storms, as in Figure 3.

2) At each level, the horizontal average of a variable Q in the hypothetical three-dimensional cloud or precipitation region is the same as obtained from the two-dimensional model.

3) Mid-levels of the slices are at grid point levels, so that contributions from the lower (j = 1) and upper (j = N) boundaries are weighted by half.

From the first assumption,

$$A_j = \pi n_j^2 \Delta x^2/8 \tag{6}$$

and from the other two assumptions,

$$I_R(Q) \doteq \Delta z \sum_j \sigma_j A_j \tilde{Q}_j \tag{7}$$

Equations (6) and (7) yield

$$I_R(Q) \doteq (\pi \Delta x^2 \Delta z/8) \sum_j [\sigma_j n_j (\sum_i Q_{i,j})] \tag{8}$$

In estimating either latent heat release or total liquid water mass (precipitation plus cloud droplets), R was taken to be the region of saturation C. In estimating total precipitation mass, R was taken to be the precipitation region P. By the method used for treating precipitation, P in this model was always within C. Throughout the time interval covered in the earlier energetics analysis, each slice for either P or C occurred in consecutive grid points, without "holes" (a small secondary cloud appearing late in the period was not counted).

The integrand Q connected with the various properties was as follows:

Latent heat release	$\rho c_p(\gamma_d - \gamma_m)w$
Mass of liquid water	L
Mass of precipitation	L_p

d. Results

Successive positions and outlines of the model cloud in Figure 8 show its evolution during a 63-minute interval from a shallow cloud assumed initially to a deep precipitating cloud with a continuously lengthening anvil. The full grid is 55 x 21, with Δx = 3.2 km and Δz = 700 m. To keep the cloud fully within the grid for a longer time than otherwise possible, the grid is shifted intermittently as described previously (Schlesinger, 1972) after the leading edge approaches the original outflow boundary sufficiently closely. In order to avoid complications due to the shifting, the detailed energetics analysis described in the above reference was confined to a 35 x 21 subregion as diagrammed in Figure 8.

In this particular experiment, precipitation commences about midway between the times shown in Figures 8c and 8d. The perturbation circulation and liquid water distribution within the cloud are shown in Figure 9 for the three time levels corresponding to Figures 8c, 8e, and 8g, with precipitation present in Figures 9b and 9c. In these two diagrams, the isolines of liquid water content should be compared with the RHI reflectivity contours for the actual Oklahoma storm in Figure 3, with the exception that the radar would not "see" the anvil since it is composed of mainly small ice particles. The model isolines are smoother than the reflectivity contours, mainly due to the rather coarse grid resolution. In both the actual and model storms, the liquid water content decreases from the cloud core outward with largest concentrations at lower or middle levels, and contours are nearly erect despite marked ambient wind shear. In the model cloud, as evident from Figure 9, release of latent heat greatly dominates evaporative cooling; the maximum updraft velocities in the cloud core in Figures 9a-9c are about 6, 11 and 10 m sec^{-1} respectively, while the downdraft near the upshear cloud edge in Figure 9c is only about 2.5 m sec^{-1}.

Figure 10 shows the time variation of latent heat release for the model storm. The graph indicates an initial rate of about 2×10^{11} cal sec^{-1} and slow development during the cumulus stage, followed by rapid intensification from around 20 minutes (just before the onset of precipitation) until about 35 minutes, then evolving to a much slower increase that continues through the remainder of the time interval. During the mature stage, the latent heat release is roughly 2.5×10^{12} cal sec^{-1}, similar to the average values near 3.5×10^{12} cal sec^{-1} estimated for the Oklahoma storm during the period 1840 through 1930 hours. The model estimate also compares favorably with values of 10^{12} to 10^{13} cal sec^{-1} estimated from geostationary satellite observations of individual severe storms occurring on 23 April 1968 in the east central United States (Sikdar et al., 1970).

For completeness, it should be noted that the latent heat release plotted in Figure 10 has been computed using horizontal averages which include weak downdrafts, with moist - adiabatic evaporation, as well as the main updraft with its condensation. Thus, referring to Equation (5), the quantity plotted corresponds to G - E, rather than G alone. However, since vertical motions in the model cloud are dominated by the main updraft, as is apparent from Figure 9, order-of-magnitude comparisons remain valid within the limitations of the assumptions underlying the estimation method.

In Figure 11, the masses for both precipitation and total liquid water are plotted. Since some liquid water drops detectable by radar may be insufficiently large to have significant relative fall speeds, the radar-detectable liquid water corresponding to the model storm might be thought of as being somewhere between the two amounts graphed. The slow increase of the latent heat release after 35 minutes has no counterpart in the total liquid water

content, which continues to increase rapidly; as of 63 minutes, its value is 1.3×10^{10} kg, which is at least an order of magnitude higher than the maximum radar-detectable liquid water for the Oklahoma storm in Figure 5. The rapid increase reflects mainly the nearly linear growth of the anvil, as seen in Figures 8e-8h, which would go undetected by a radar. In the model storm, about 2×10^{8} kg of precipitation forms instantaneously near 22 minutes as the cloud top first penetrates the -20C level. The precipitation mass increases throughout the remainder of the time interval shown, but much more slowly than the total liquid water mass during maturity. At the end of the interval, the model storm contains slightly over 10^{9} kg of precipitation. The radar-detectable liquid water content for the Oklahoma storm shows a maximum of 5.7×10^{8} kg at the peak intensity of the storm. These very close agreements in results between the observed storm and the model storm should not be regarded as merely fortuitous because (1) they approximate each other in overall dimensions and (2) similar results in latent heat release have been calculated for thunderstorms observed by geostationary satellites (Sikdar et al., 1970).

It is only fair to note that the treatment of water substance in the numerical model, in particular the last of the four assumptions noted earlier, leads to some admittedly unrealistic features. Precipitation is everywhere accompanied by 1 gm m^{-3} of cloud droplets, with saturated air, and cannot fall out of the cloud base without completely evaporating. Surface rainfall is preceded by descent of the cloud base to the ground. This is in contrast to actual thunderstorms, which commonly feature a well-defined cloud base from which heavy precipitation may reach the ground without saturating the air, perhaps even accompanied by a decrease in surface relative humidity (Byers and Braham, 1949). The omission of the ice phase latent heat is not regarded as a major drawback in the present context, since the same simplifying assumption

was made in estimating parameters in the Oklahoma storm.

As already noted, the extension to elliptical horizontal cloud layers from plane cross-sections departs from the rectilinear geometry of the model, originally designed for simulating roll-type convection. In this context, the estimates of latent heat release and liquid water content presented here should be regarded cautiously, in light of recent numerical cloud modeling results obtained by Soong and Ogura (1972) and Murray (1970).

In these cases, two experiments were run, one using axial symmetry and the other using slab symmetry. Both geometries used identical base states, initial perturbations, governing equations and boundary conditions. Soong and Ogura, as well as Murray, found that the axially symmetric cloud developed more vigorously than the slab-symmetric cloud. A stronger updraft, and in turn more liquid water production, resulted. Along the axis of symmetry, the maximum rainwater content in the precipitating model of Soong and Ogura was about half as great for the slab-symmetric cloud; the corresponding ratio for cloud water in Murray's non-precipitating model was only about 1:4. Maximum updraft velocities showed similar contrasts.

This suggests that the estimates of cloud-integrated liquid water content and latent heat release in the model storm might be conservative, since they are generated from a rectilinear two-dimensional model and the cylindrical geometry better approximates three-dimensionality than the rectilinear geometry. However, the areal proportion of a horizontal cloud slice occupied by the active core is larger in the rectilinear geometry than in the cylindrical geometry, thereby weighting the core contributions to horizontal averages more strongly. Hence, assuming equal horizontal averages for a rectangular model cloud slice and for the elliptical wafer generated from it should tend

to counteract the tendency of a relatively weak storm core to limit the magnitudes of the integrals involved.

The smooth time variations in Figure 10 and 11 should be contrasted with the more irregular variations shown in Figure 5 and 6 for the Oklahoma storm. Computationally produced pseudo-diffusion (Schlesinger, 1972) may be partly responsible. Also, the omission of the ice phase precludes hail, and the model cannot resolve such small features as tornadoes. Nevertheless, the reasonable magnitudes of the estimated latent heat release and liquid water content in the model storm suggest that the model possesses a useful degree of realism in spite of these limitations.

6. Concluding Remarks

In this paper, the time variation of mass-integrated liquid water content and latent heat release for a severe thunderstorm in pronounced vertical shear has been investigated in two phases. An actual storm in Oklahoma has been analyzed, and the observed magnitudes have then been compared with those estimated from a previous two-dimensional numerical modeling experiment (Schlesinger, 1972).

a. Summary of procedure

Radar reflectivity profiles have provided the main source of data for the Oklahoma storm. An approximate continuity equation (Holtz, 1968) for time variation of liquid water is applied, along with the Gunn-Marshall equation for reflectivity versus liquid water content and an empirical relationship (McLaughlin, 1967) between rainfall rate and downdraft evaporation rate. Reflectivity contours are treated as cylindrical shells to simplify computations, and the ice phase is ignored.

The two-dimensional model cloud is extended systematically to a three-dimensional region by assuming elliptical horizontal cross-sections reasonably approximating observed shapes for cloud and precipitation regions. Horizontal averages of integrands at each level are assumed equal to those generated by the model, without any specific assumptions on point-by-point variations.

The Oklahoma storm has been analyzed over about 120 minutes beginning with the late growth state. In partial contrast, the model simulates slightly over 60 minutes in the life cycle of a convective cloud, from the early growth stage to the peak of maturity. Ice is not explicitly included in the model, with liquid water being partitioned into cloud droplets and precipitation following Takeda (1966).

b. Principal conclusions

1) For the Oklahoma storm, both latent heat release and radar-detectable liquid water content are found to maintain the same order of magnitude during maturity, despite fluctuations apparently associated with a funnel cloud and surface hail. Latent heat release ranges between about 2 and 8 x 10^{12} cal sec^{-1}, while liquid water content is between 1 and 5 x 10^{8} kg.

2) Both the liquid water mass and the latent heat release are at least an order of magnitude greater for the Oklahoma storm than the values estimated for airmass thunderstorms by Braham (1952).

3) From an initial value near 2 x 10^{11} cal sec^{-1}, latent heat release in the model storm increases to about 2.5 x 10^{12} cal sec^{-1} by 35 minutes and is then steady or only slightly increasing through 63 minutes. Total liquid water content increases by an order of magnitude during this mature phase, nearly as rapidly as in the preceding 35 minutes, reaching 10^{10} kg at the end of the interval. Precipitation content, presumably a closer analogue of radar-detectable liquid water, increases considerably more slowly during maturity and shows signs of leveling off near 10^{9} kg.

4) Thus, in the mature phase, both the actual storm and the model storm exhibit comparable values for latent heat release as well as radar-detectable liquid water, identifying the latter with precipitation particles. Omission of the ice phase from consideration in both analyses is presumably not a major error, since the heat of vaporization is about 7.5 times the heat of fusion and orders of magnitude are of more interest here than accurate values.

5) The model yields smoother time variation and liquid water reflectivity contours than the actual storm. This is considered to be largely due to limited spatial resolution in the model, precluding representation of such small observed features as tornadoes or echo-free notches.

Acknowledgements

The preliminary research reported in this paper was performed in phase I of the continuing studies on energetics of hail storms supported by the National Science Foundation under NSF grant GI-31278X. The courtesy of Mr. J. T. Dooley of the National Severe Storm Laboratory in supplying the observational data used in this study is much appreciated. Thanks are also due to Mr. Gary Ellrod for computing some of the data reported in this paper.

Figure Legends

Figure 1 A scheme for computing liquid water content from RHI reflectivity profiles.

Figure 2 Storm track as viewed from the NSSL radar.

Figure 3 A sample of PPI and RHI reflectivity profiles of the storm investigated. Reflectivity values are in steps of 10 dbz increasing towards storm center with the outermost one representing 10 dbz.

Figure 4 Time variations of rainfall rate estimated from radar reflectivity data.

Figure 5 Time variations of total liquid water content as derived from the RHI profiles.

Figure 6 Time variations of: (a) the generation rate, and (b) latent heat release.

Figure 7 Construction of hypothetical cross-sections for estimating mass-integrated quantities from the two-dimensional numerical model.

Figure 8 Successive outlines and positions of the model cloud, full 55-by-21 grid and 35-by-21 subregion (see text) relative to the earth's surface. Boundaries are given by thick solid lines for the subregion, thick dashed lines for the remainder of the grid, and thin solid curves for the cloud. (a) Initial time, no grid shifts; (b) 9.0 min, no grid shifts; (c) 18.5 min, no grid shifts; (d) 27.5 min, no grid shifts; (e) 36.1 min, no grid shifts; (f) 45.3 min, 6 grid shifts; (g) 54.4 min, 14 grid shifts; (h) 63.0 min, 20 grid shifts.

Figure 9 Convection in the 35-by-21 subregion at: (a) 18.5 min, (b) 36.1 min, (c) 54.4 min. The cloud is indicated by shading. Thin solid curves with arrows are streamlines for the deviation of the flow from the base state, and are contoured at intervals of 10^7 gm m^{-1} sec^{-1}. Thick solid curves are isolines of liquid water content L (gm m^{-3}).

Figure 10 Time variations of latent heat release estimated from the numerical model.

Figure 11 Time variations of total liquid water content and precipitation content estimated from the numerical model.

References

Barge, B., 1968: Thunderstorm energy budgets from radar. Proc. Thirteenth Radar Conf., Am. Met. Soc., Boston.

Barnes, S. L., et al., 1971: "Rawinsonde observation and processing techniques at the NSSL." NOAA Tech. Memo. ERL NSSL-53, 246 pp.

Braham, R., 1952: The water and energy budgets of the thunderstorm and their relation to thunderstorm development. J. Meteor. 9, 227-242.

Brown, R. A., 1967: Mass and available energy in growing convective clouds. J. Atm. Sci., 24, 308-311.

Byers, H. and R. Braham, 1949: The thunderstorm, U. S. Dept. of Commerce.

Fankhauser, J., 1971: Thunderstorm-environmental interactions determined from aircraft and radar observations. Mon. Wea. Rev., 99, 171-192.

Geotis, S. G., 1971: Thunderstorm water contents and rain fluxes deduced from radar. J. Appl. Meteor., 10, 1233-1237.

Gunn, K. L. S., and J. S. Marshall, 1958: The distribution with size of aggregate snowflakes. J. Meteor., 15, 452-461.

Holtz, C. D., 1968: Life cycle of a summer storm from radar records. Report MW-55, McGill Univ., Montreal, 46 pp.

Marwitz, J., 1972: The structure and motion of severe hailstorms. Part I: Supercell storms. J. Appl. Meteor., 11, 166-179.

McLaughlin, M. R., 1967: The energy budget of a severe local storm, Rep. #7, Univ. of Texas, Austin, 55 pp.

Murray, F. W., 1970: Numerical models of a tropical cumulus cloud with bilateral and axial symmetry, Mon. Wea. Rev., 98, 14-28.

Murray, F. W., and C. E. Anderson, 1965: Numerical simulation of the evolution of cumulus towers. Douglas Report SM-49230, Missile & Space Systems Division, Santa Monica, California.

Schlesinger, R. E., 1972: An investigation into the energetics of severe local storms using a two-dimensional numerical model, Report 72-1, University of Wisconsin, Madison, 54 pp.

Sikdar, D. N., V. E. Suomi and C. E. Anderson, 1970: Convective transport of mass and energy in severe storms over the United States - An estimate from a geostationary altitude. Tellus 22, 521-532.

Soong, S. and Y. Ogura, 1972: A comparison between axisymmetric and slab-symmetric cumulus cloud models, Convection Series 72-6, University of Illinois.

Takeda, T., 1966: Effects of the prevailing wind with vertical shear on the convective cloud accompanied with heavy rainfall. J. Meteor. Soc. Japan, 44, 129-144.

Wilson, J. W., 1969: Radar measurements of rainfall for operational purposes. Final report 7488-360 on contract E 22-23-69(N), Travelers Research Corp., Hartford, Conn., 44 pp.

U. S. Dept. of Commerce, 1968: Storm Data Vol. 10, No. 5.

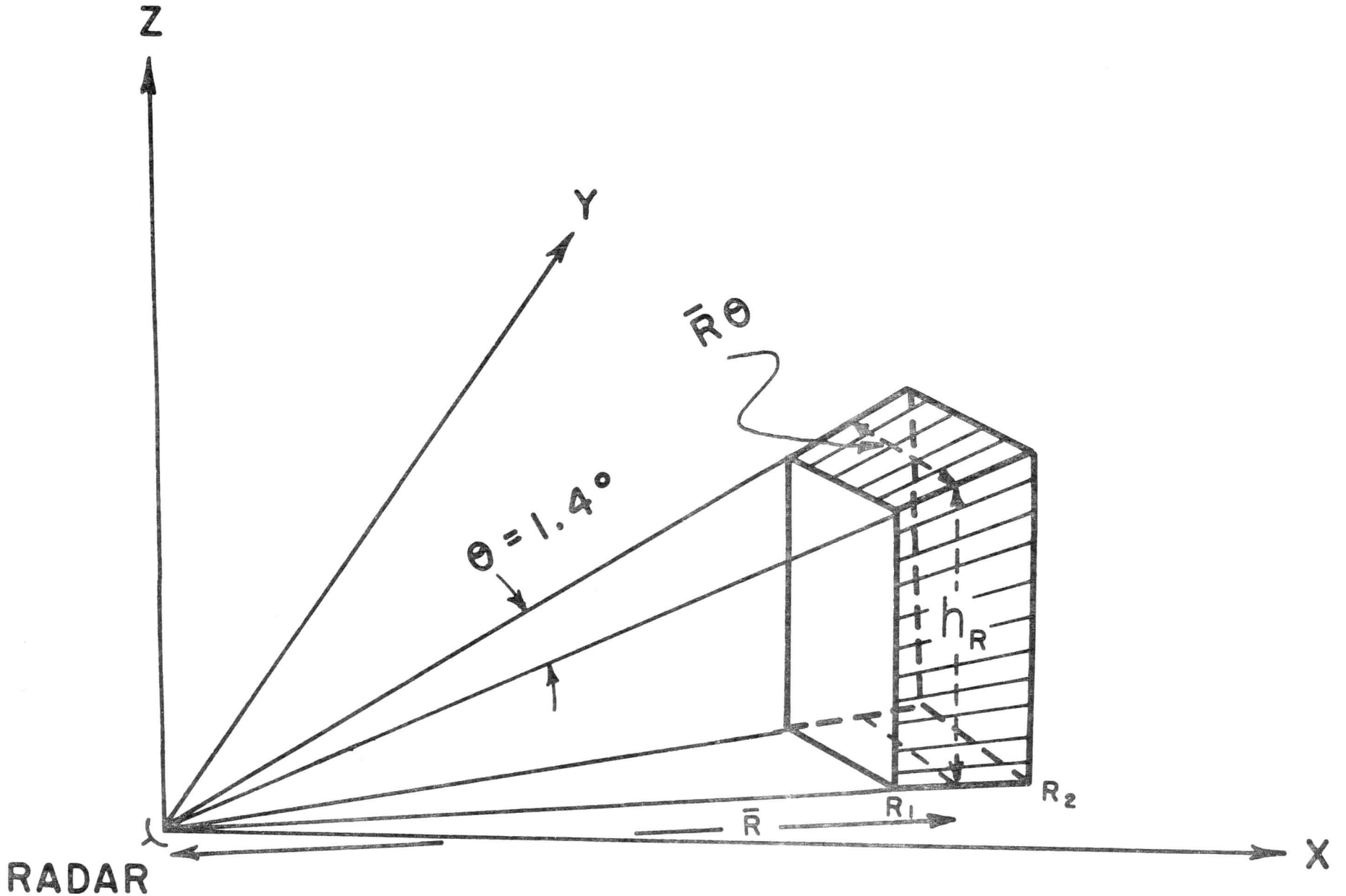
Z
Y
$\bar{R}\theta$
$\theta = 1.4°$
h_R
R_2
R_1
$\bar{R}$
X
RADAR

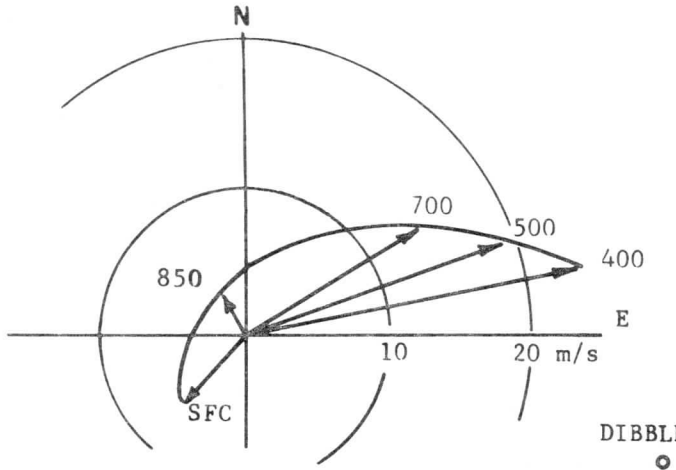

WINDS ALOFT AT DIBBLE, OKLA.
1900 - 1930 CST

PPI

1835 C 1855 C 1910 C 1930 C 1945 C

RHI

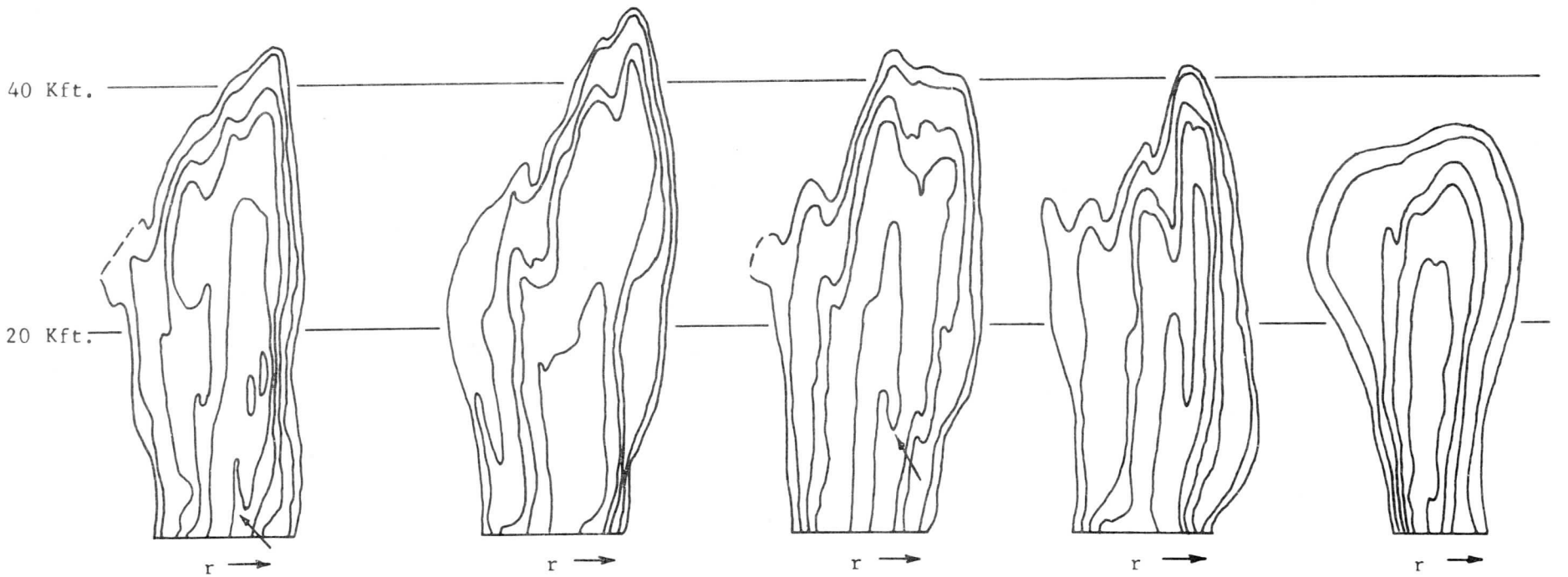

1835 C, 187°azi. 1907 C, 167°azi. 1920 C, 163°azi. 1937 C, 157°azi. 2005 C, 154°azi.

SCALE: r= 10 NM

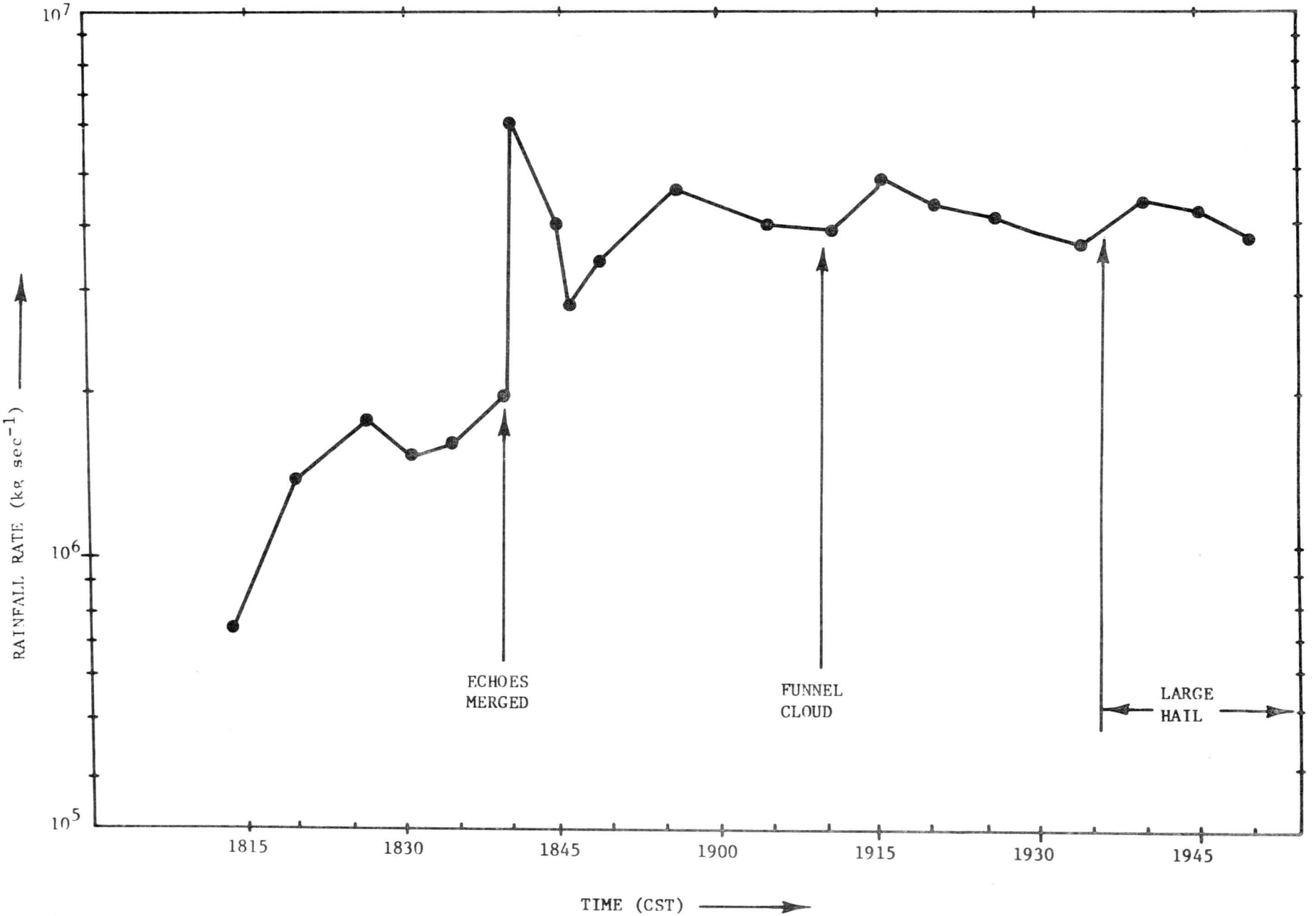
10^7
10^6
10^5
RAINFALL RATE (kg sec^{-1})
ECHOES MERGED
FUNNEL CLOUD
LARGE HAIL
1815
1830
1845
1900
1915
1930
1945
TIME (CST)

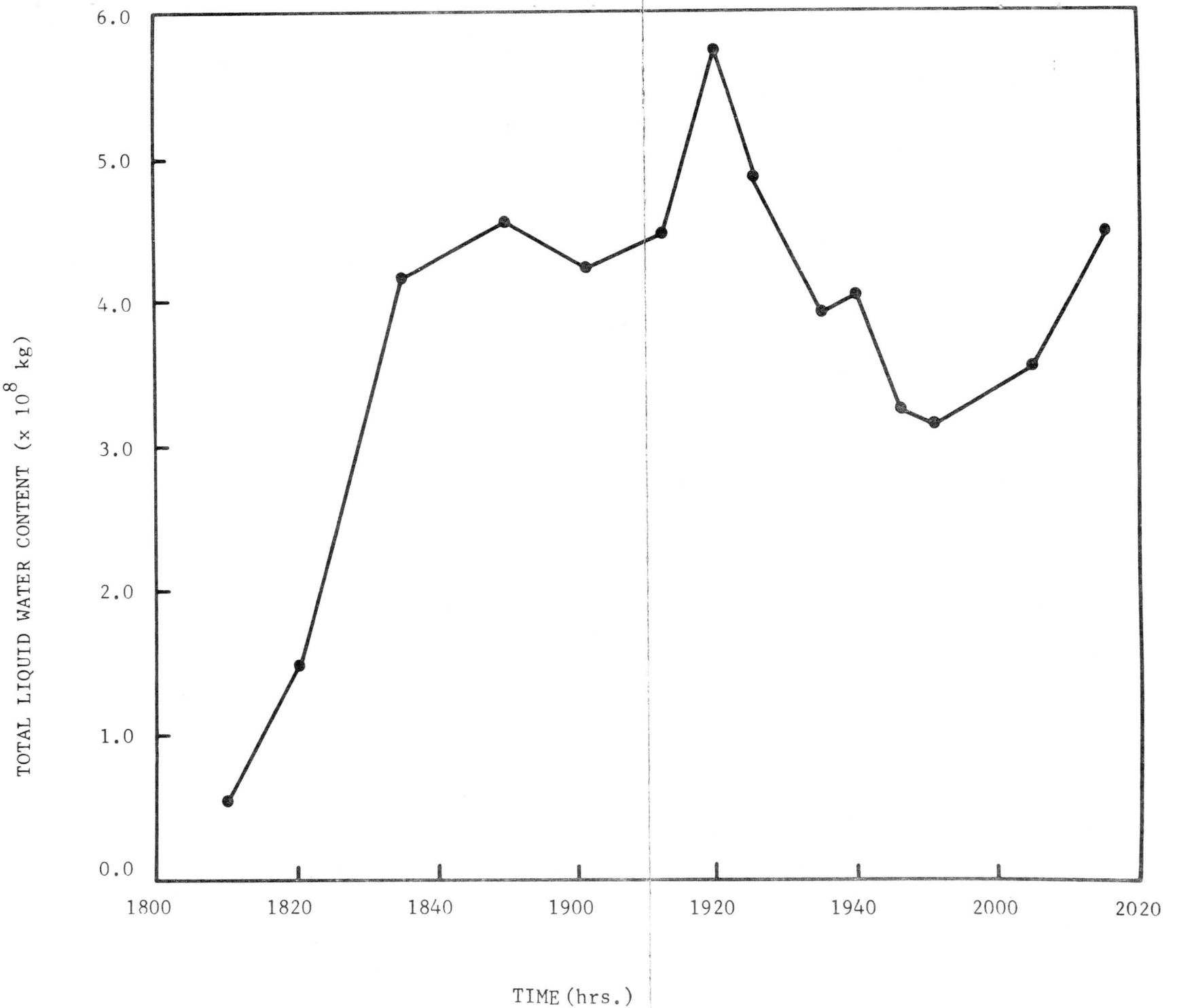
6.0
5.0
4.0
3.0
2.0
1.0
0.0
TOTAL LIQUID WATER CONTENT (x 10^8 kg)
1800
1820
1840
1900
1920
1940
2000
2020
TIME (hrs.)

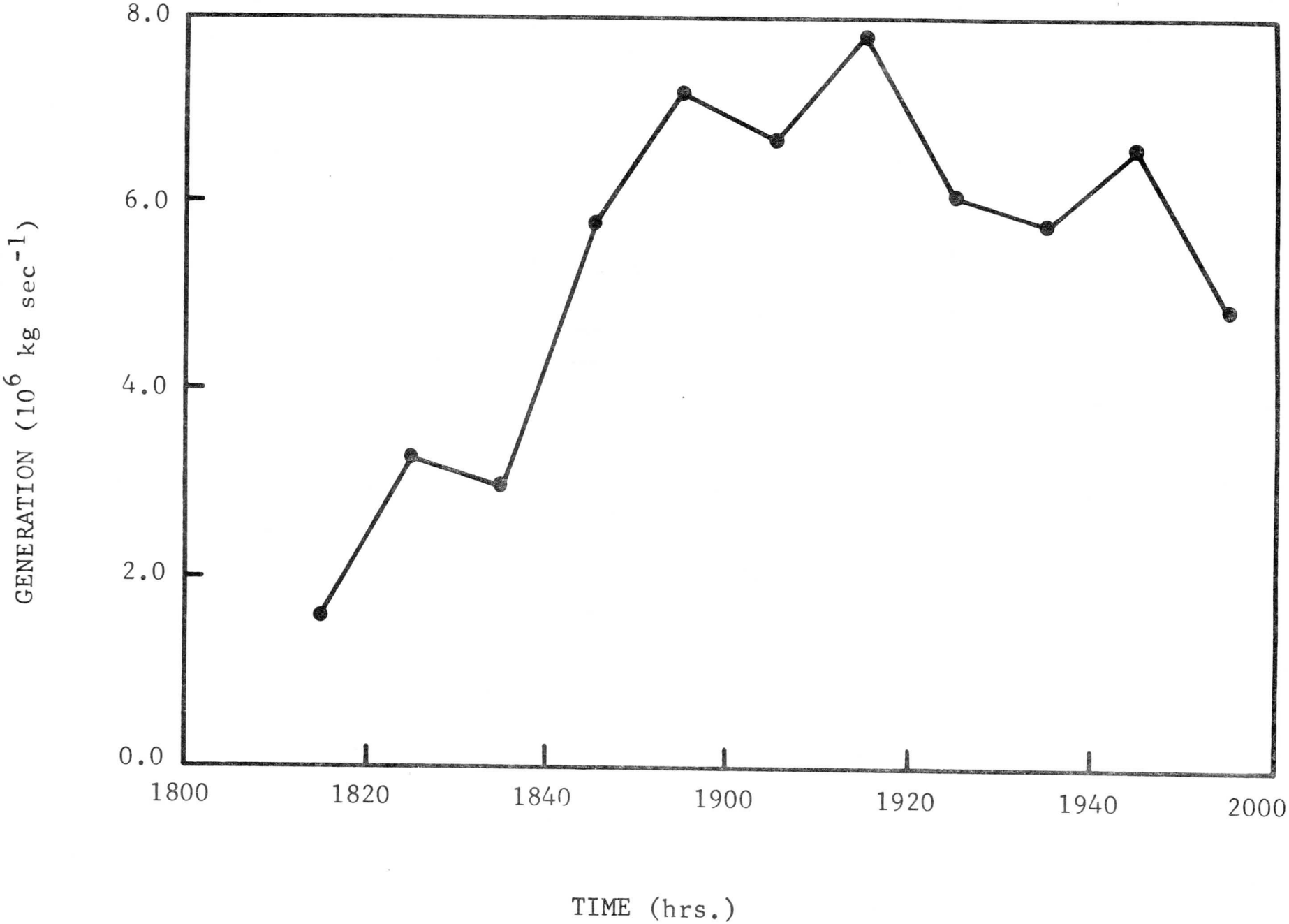
8.0
6.0
4.0
2.0
0.0
GENERATION (10^6 kg sec^{-1})
1800
1820
1840
1900
1920
1940
2000
TIME (hrs.)

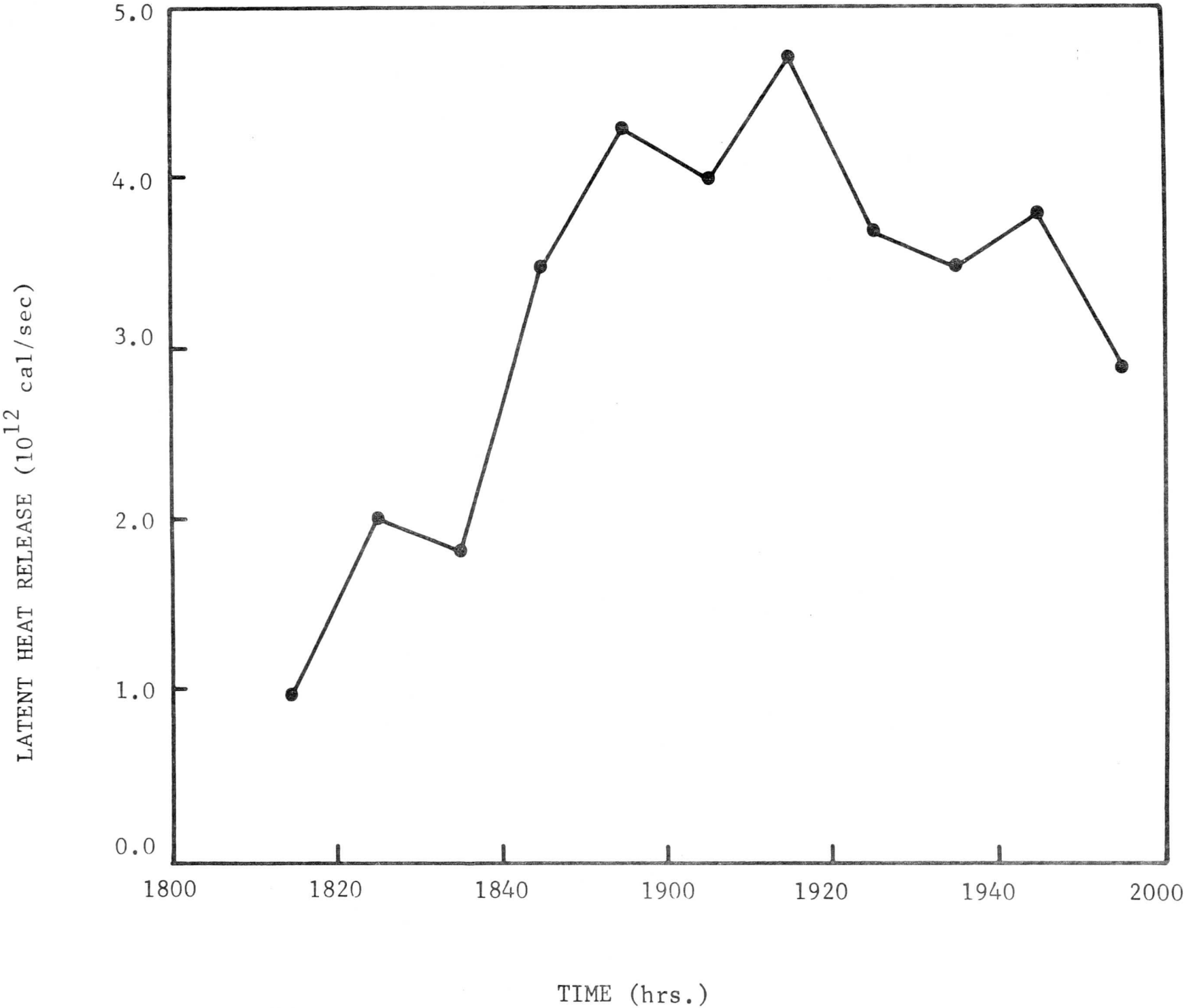
5.0
4.0
3.0
2.0
1.0
0.0
LATENT HEAT RELEASE (10^{12} cal/sec)
1800
1820
1840
1900
1920
1940
2000
TIME (hrs.)

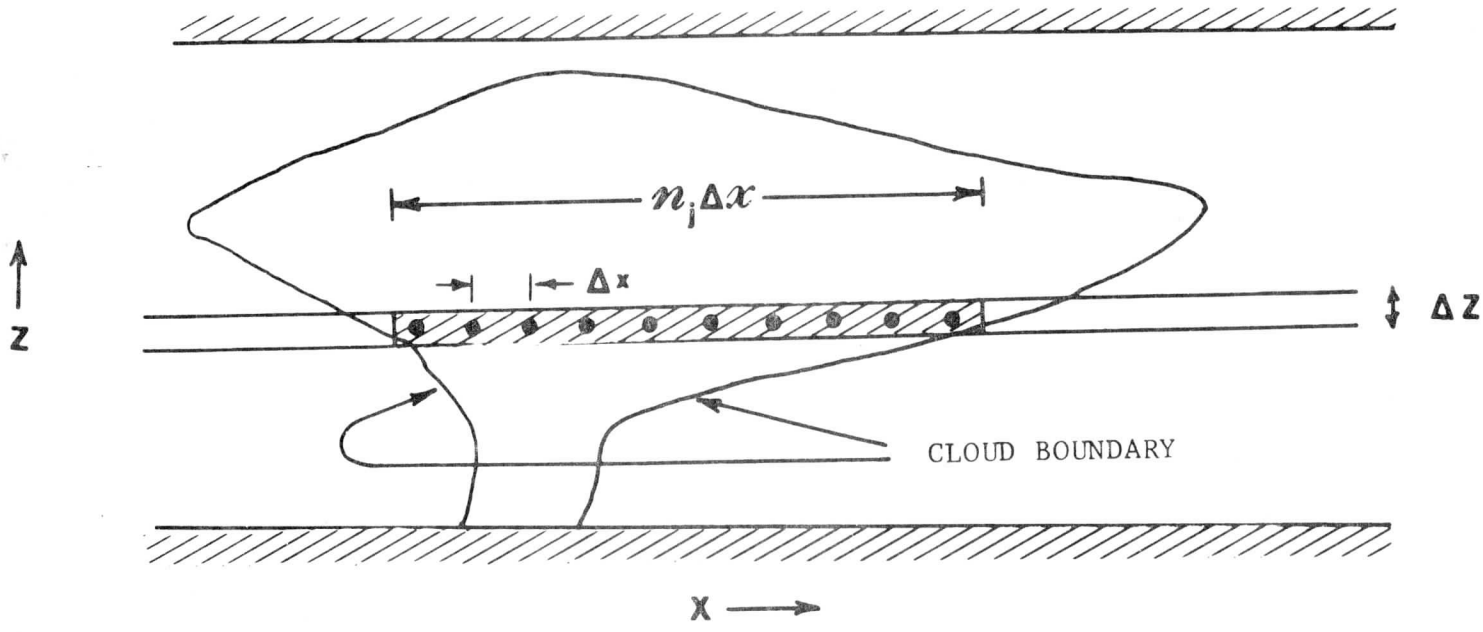

TYPICAL CLOUD SLICE
IN MODEL PLANE

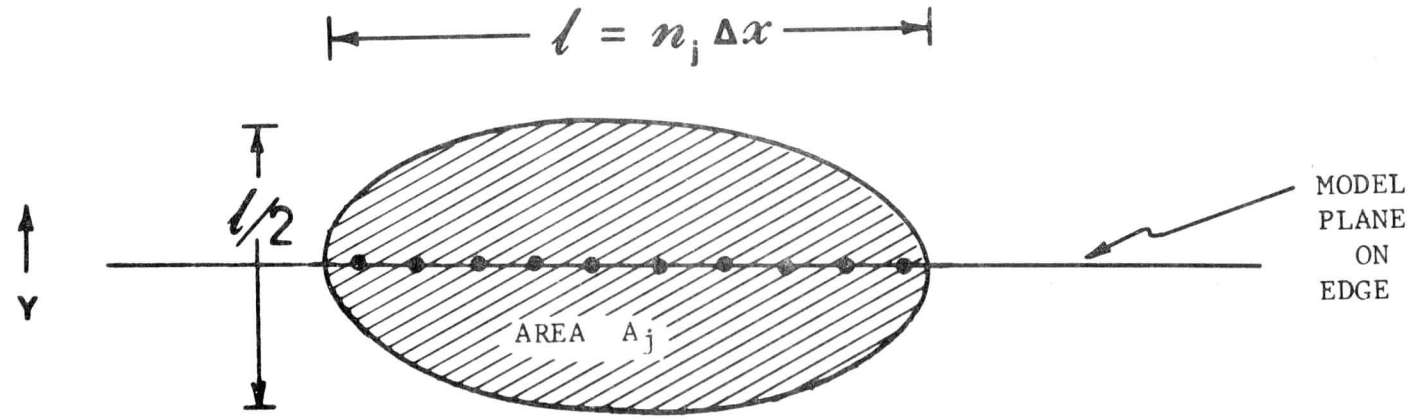

HYPOTHETICAL
HORIZONTAL CROSS-SECTION
GENERATED FROM SLICE

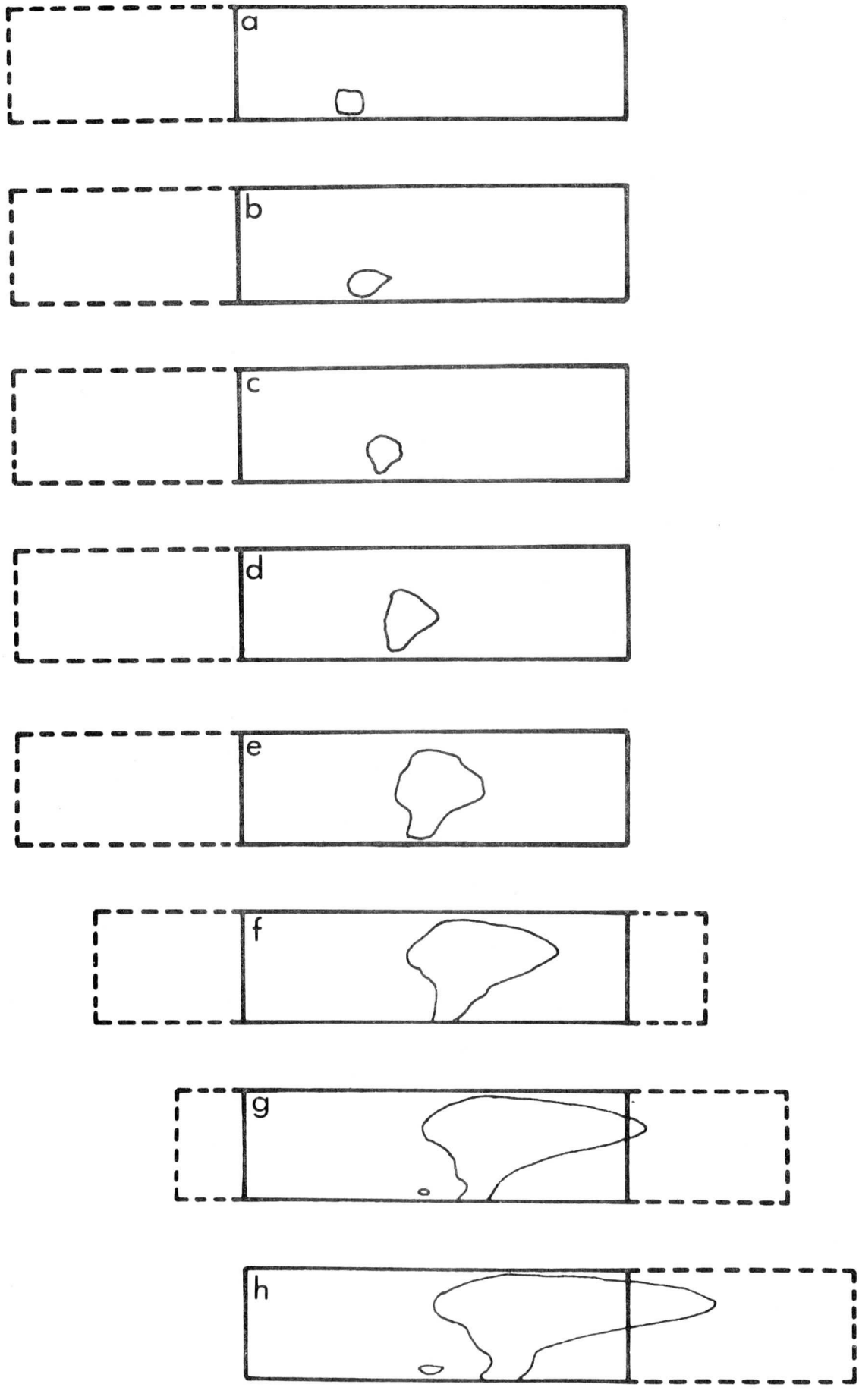
a
b
c
d
e
f
g
h

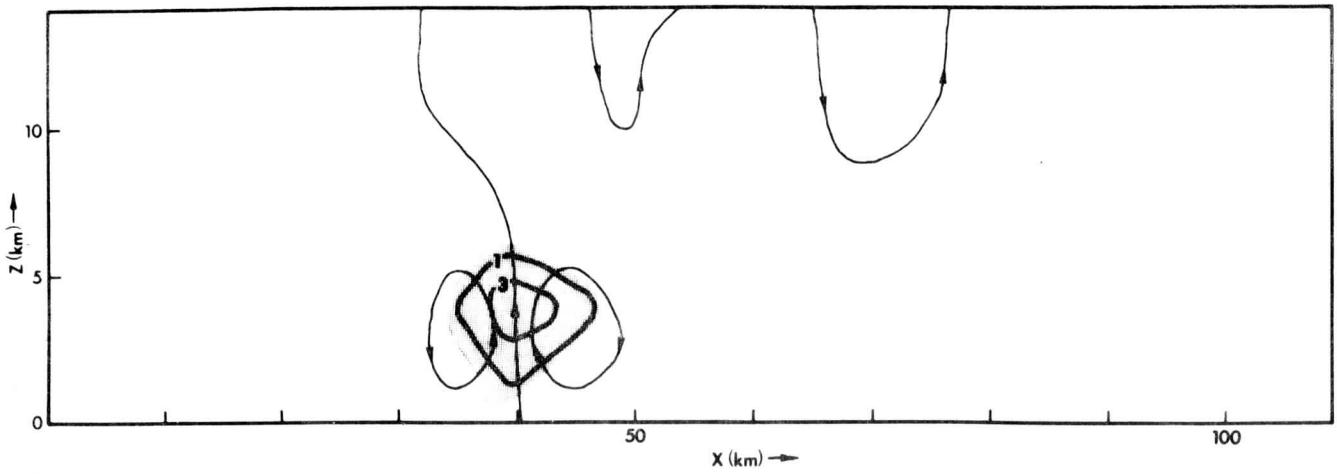
10
5
0
Z (km)
1
3
50
100
X (km)

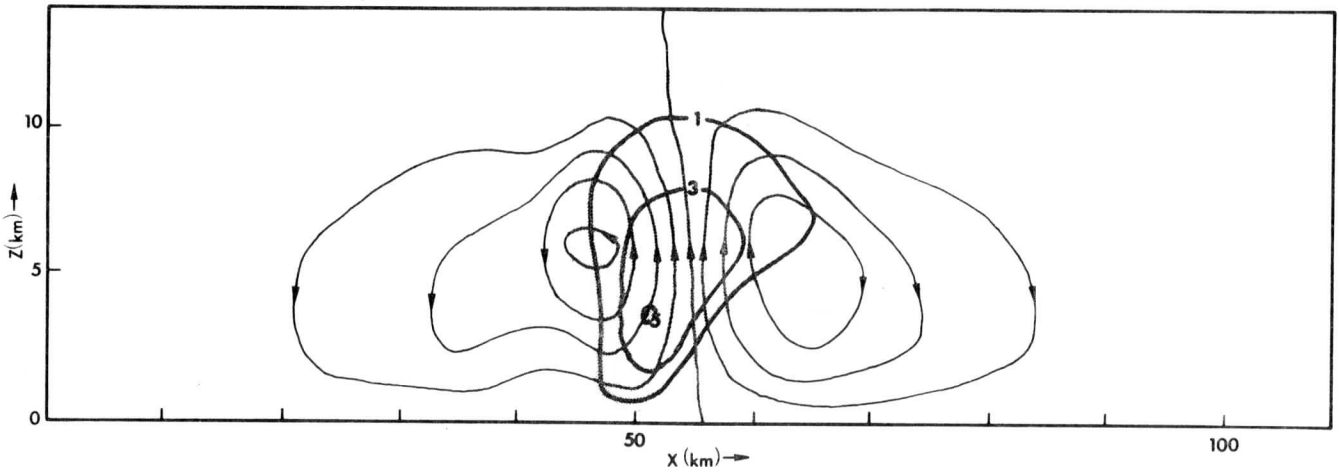
10
5
0
Z(km)
1
3
50
100
X (km)

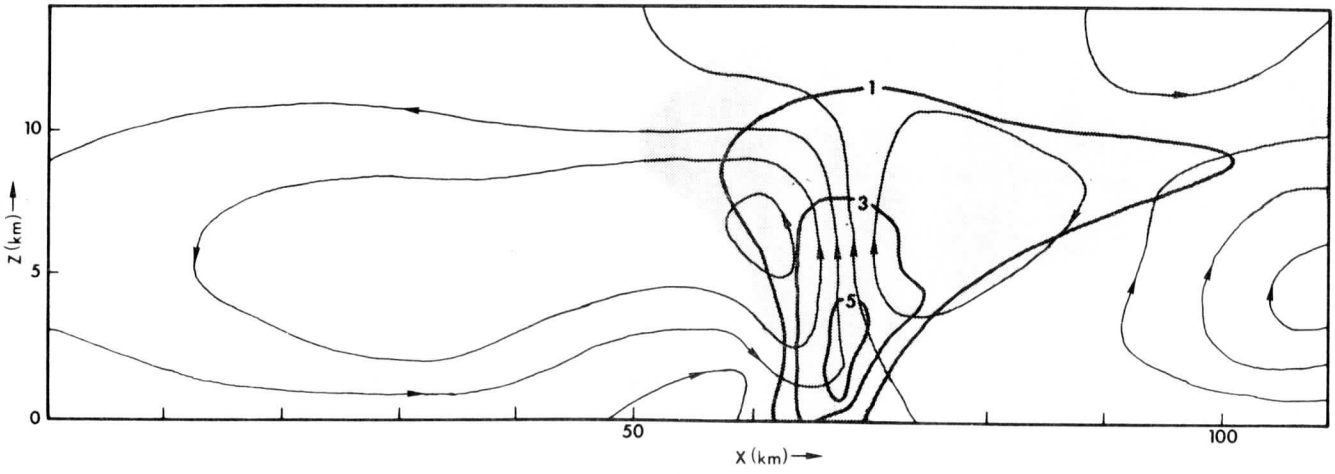
10
5
0
Z (km)
1
3
5
50
100
X (km)

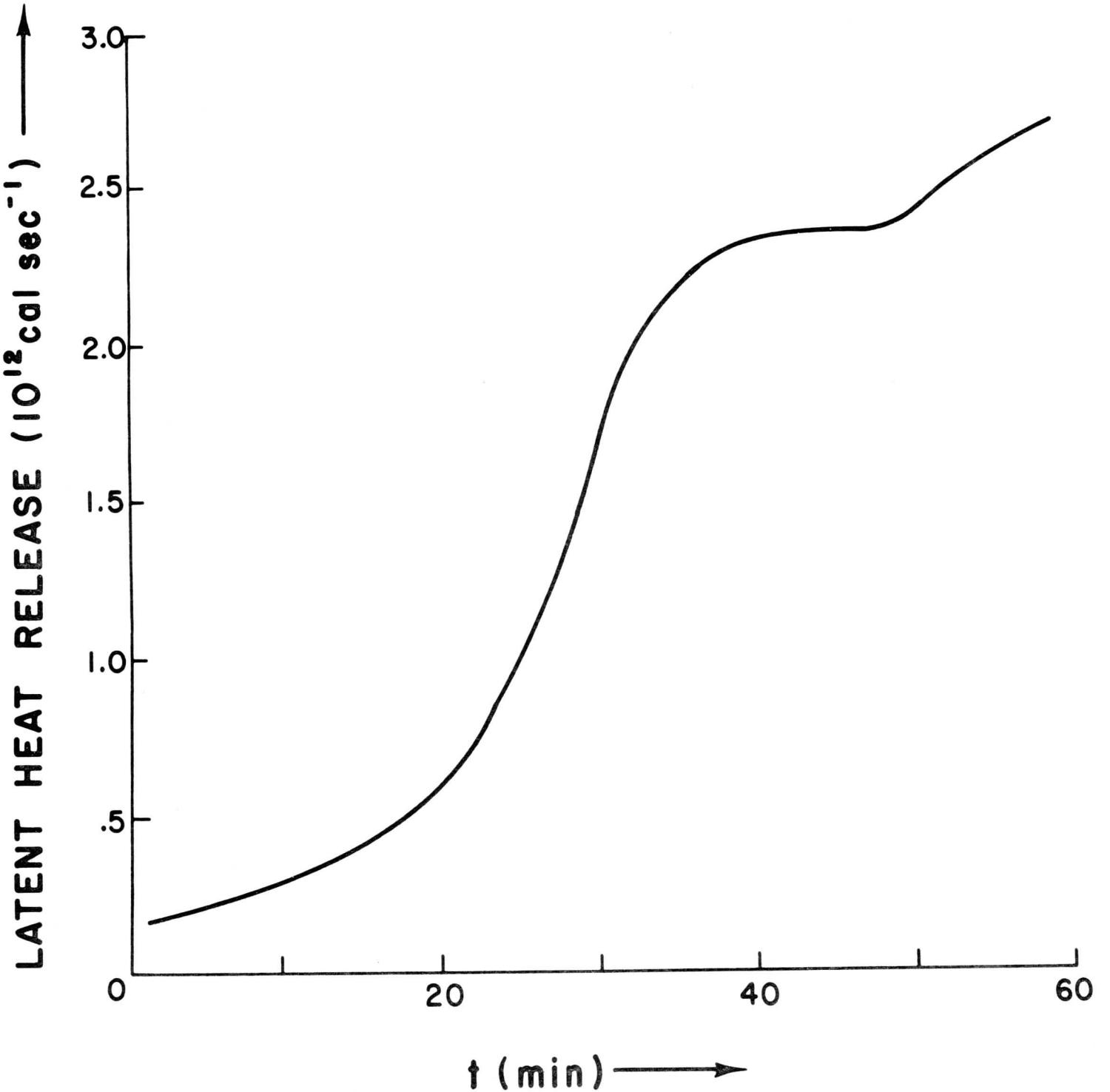
LATENT HEAT RELEASE (10^{12}cal sec^{-1})
3.0
2.5
2.0
1.5
1.0
.5
0
20
40
60
t (min)

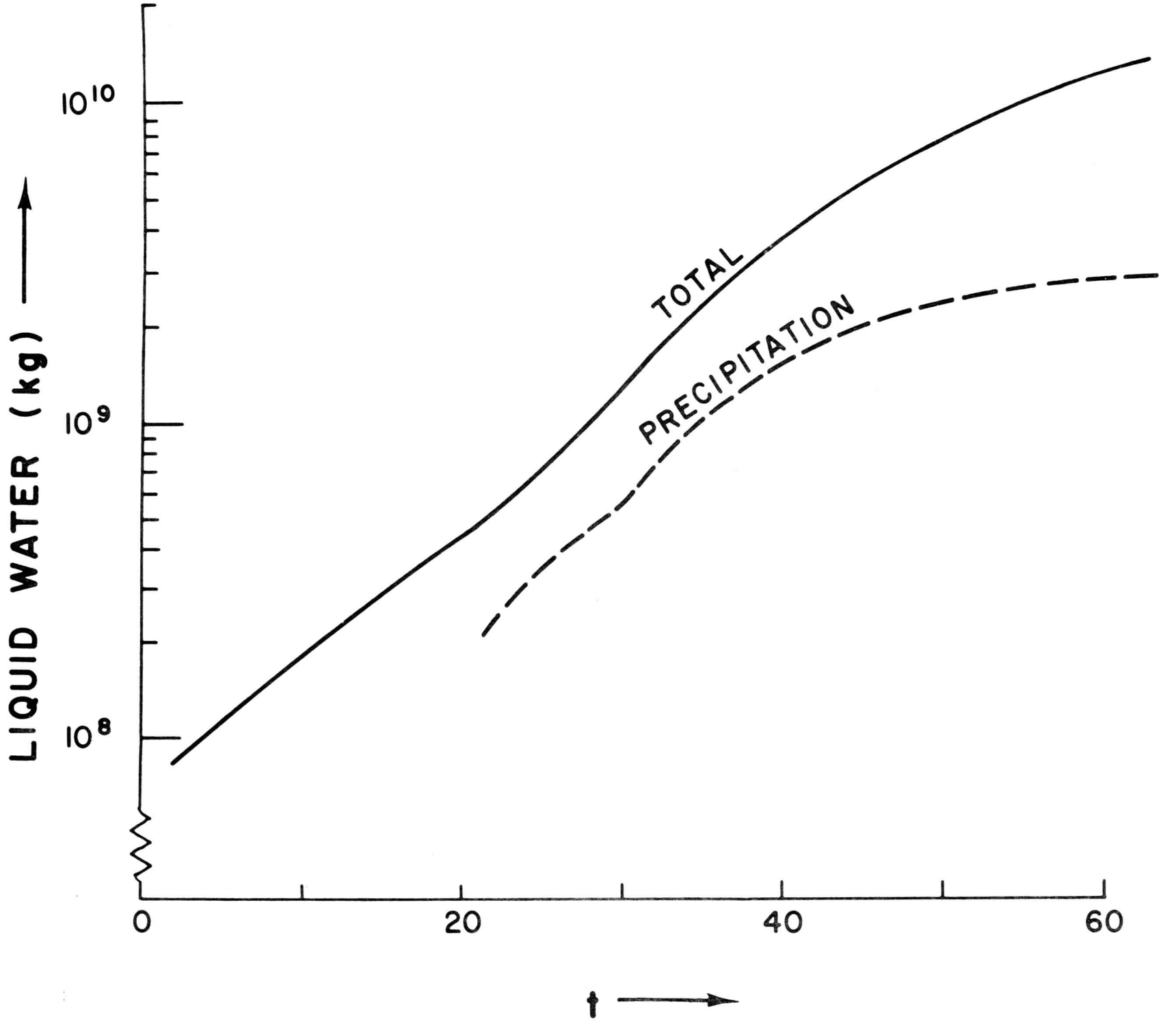
LIQUID WATER (kg)
10^{10}
10^{9}
10^{8}
TOTAL
PRECIPITATION
0
20
40
60
t